RSC Advances

PAPER

View Article Online
View Journal | View Issue

Cite this: *RSC Adv.*, 2023, **13**, 9491

Carbon dot incorporated mesoporous silica nanoparticles for targeted cancer therapy and fluorescence imaging†

Abolghasem Abbasi Kajani, *[a] Laleh Rafiee,[b] Shaghayegh Haghjooy Javanmard,[b] Nasim Dana[b] and Setareh Jandaghian[b]

Received 4th February 2023
Accepted 17th March 2023

DOI: 10.1039/d3ra00768e

rsc.li/rsc-advances

A new and efficient theranostic nanoplatform was developed *via* a green approach for targeted cancer therapy and fluorescence imaging, without the use of any anticancer chemotherapeutic drugs. Toward this aim, monodisperse and spherical mesoporous silica nanoparticles (MSNs) of approximately 50 nm diameter were first synthesized using the sol–gel method and loaded with hydrothermally synthesized anticancer carbon dots (CDs). The resulting MSNs-CDs were then functionalized with chitosan and targeted by an anti-MUC1 aptamer, using the glutaraldehyde cross-linker, and fully characterized by TEM, FE-SEM, EDS, FTIR, TGA, XRD, and BET analysis. Potent and selective anticancer activity was obtained against MCF-7 and MDA-MB-231 cancer cells with the maximum cell mortalities of 66.2 ± 1.97 and 71.8 ± 3%, respectively, after 48 h exposure with 100 μg mL^{-1} of the functionalized MSNs-CDs. The maximum mortality of 40.66 ± 1.3% of normal HUVEC cells was obtained under the same conditions. Based on the results of flowcytometry analysis, the apoptotic mediated cell death was recognized as the main anticancer mechanism of the MSNs-CDs. The fluorescence imaging of MCF-7 cancer cells was also studied after exposure with MSNs-CDs. The overall results indicated the high potential of the developed nanoplatform for targeted cancer theranostics.

1. Introduction

Cancer has been reported as the second lethal disease with about 10 million global victim in 2020.[1] Despite the significant advances over the past decades, the early detection and efficient therapy of cancer still remain important challenges.[2] Most of the commonly used cancer detection methods are not specific and sensitive enough to accurately diagnose the early stages of disease.[3] On the other hand, the conventional methods of cancer therapy, including surgery, radiation, and chemotherapy, are not efficient and usually lead to significant side effects.[4] Therefore, the development of specific and efficient approaches are necessary to overcome the present obstacles of cancer detection and therapy.[5]

The nano-based approaches have promising potential in both fields of cancer detection and treatment.[6] The attractive physicochemical properties of nanoparticles (NPs) such as size, optical properties, magnetic activity, high surface to volume ratio, and high surface activity, are extensively used for different biomedical applications.[7] The nanoscale carriers are of great interest for drug delivery due to their high stability, facile chemical functionality, efficient cellular internalization, and high loading capacity.[8] Development of smart and multifunctional nanoplatforms with different surface chemistry and novel abilities has also considered, recently.[9] In this context, the surface functionalization by the targeting agents, especially antibodies and aptamers, have greatly considered for the targeted delivery of nanocarriers with high efficiency and specificity.[10] The design and development of theranostic nanoplatforms for simultaneous diagnosis and therapy of diseases is another outstanding achievement of nanotechnology.[11]

A plenty of NPs with different sizes, shapes and physicochemical properties have been developed so far for various biomedical applications.[12] Among them, mesoporous silica nanoparticles (MSNs) have been widely used as the nanocarrier due to their interesting characteristics, especially facile synthesis and functionalization, excellent biocompatibility, and high loading capacity.[13–17] MSNs are also considered greatly as an appropriate candidate to develop the theranostic agents.[18] Different drugs and imaging modalities have been incorporated into MSNs to achieve this goal. Carbon dots (CDs) are among the latest developed fluorescent NPs that are easily synthesized from the organic sources and used for different applications,

[a]*Department of Biotechnology, Faculty of Biological Sciences and Technology, University of Isfahan, Isfahan, 81746-73441, Iran. E-mail: agh.abbasi@bio.ui.ac.ir; Fax: +98-3137932456; Tel: +98-3137934401*

[b]*Applied Physiology Research Center, Cardiovascular Research Institute, Isfahan University of Medical Sciences, Isfahan, 81746-73461, Iran*

† Electronic supplementary information (ESI) available. See DOI: https://doi.org/10.1039/d3ra00768e

especially bioimaging.[19,20] CDs represent different functional groups such as amine, hydroxyl, and carboxyl, which facilitates their subsequent surface modification. Recently, the fluorescent CDs with potent anticancer activity have also been synthesized by our group *via* a green chemistry approach by using the extracted taxanes from *Taxus baccata* L.[21] However, the small size of CDs inhibits their direct *in vivo* applications due to their rapid renal clearance.[22] Therefore, development of appropriate nanoplatforms is fundamental for efficient and targeted delivery of CDs *in vivo*.

In the present study, MSNs were synthesized and loaded with the fluorescent and anticancer CDs to develop a new theranostic nanoplatform. After chitosan (Ch) coating and aptamer targeting, the final nanoplatforms were used, as a theranostic agent, for the fluorescence imaging and the targeted cancer therapy. Recently, many articles have been reported about the CDs and silica nanocomposites for various applications, including biosensing, bioimaging and theranostics.[23] Unlike the similar theranostic nanosystems that have been developed until now based on the combined use of CDs and chemotherapeutic agents,[24–27] the present nanoplatforms only carry CDs, as both anticancer and fluorescent agents, with a potent and comparable anticancer activity. Moreover, unlike some recent articles[28,29] that reported the photo-induced cytotoxicity of CDs, the focus of present study is the selected and targeted anticancer activity without the need for the special stimuli. The use of taxane compounds extracted from *Taxus baccata* L., as a natural and easily available source, for the synthesis of hydrophilic and fluorescent CDs, considerably reduces the common issues of chemotherapeutics, including their side effects, hydrophobicity and high costs. Moreover, the used procedure in this study for development of the theranostic nanoplatforms is simple and green without the use of complex experimental procedures or toxic chemicals.

2. Experimental section

2.1. Materials

RPMI1640 medium, 0.25% (w/v) trypsin-0.03% (w/v) EDTA solution, fetal bovine serum (FBS), phosphate-buffered saline (PBS), and antibiotic solution (penicillin–streptomycin) were prepared from Gibco (Invitrogen, Grand Island, NY). Annexin V-FITC conjugate, cell staining buffer, and annexin V binding buffer were purchased from Biolegend (San Diego, CA). 3-(4,5-Dimethylthiazol-2-yl)-2,5-diphenyltetrazolium bromide (MTT), 5-fluorouracil (5-FU), acetic acid (99%), low molecular weight (LMW) Ch, glucose ($C_6H_{12}O_6$), dimethyl sulfoxide (DMSO), cetyltrimethylammonium bromide (CTAB), tetraethyl orthosilicate (TEOS), *m*-phenylenediamine (*m*PDA) were purchased from Sigma (Sigma-Aldrich, Germany). Sodium hydroxide, glutaraldehyde (GA), absolute ethanol, and anhydrous methanol were purchased from Merck (Darmstadt, Germany). The amino-labeled anti-MUC1 aptamer was obtained from Metabion (Germany) with the previously reported sequence of 5′ NH_2C_6-TTTGCAGTTGATCCTTTGGATACCCTGG 3′.[30] The breast cancer cell lines of MCF-7 and MDA-MB-231 were acquired from the national cell bank of Iran-Pasteur Institute.

2.2. Synthesis of nanoplatforms

This section includes several steps. First, CDs were synthesized based on the previously reported hydrothermal method.[21] Briefly, 20 mL ethanolic extract of *Taxus baccata* containing *m*PDA (in a 3 : 1 w/w ratio) was prepared and added into a Teflon-lined autoclave and heated at 150 °C for 6 h. The impurities and large particles were removed by centrifugation at 8000 rpm for 10 min. Second, MSNs were synthesized according to the previously reported method by some modification.[31] 200 mg CTAB was dissolved in 96 mL of deionized water under vigorous stirring for 20 min at 80 °C. Then 70 μL of 2 M NaOH and 500 μL of TEOS were consecutively added into the solution dropwise and the solution was stirred for 2 h. The resulted MSNs were separated from the colloid by centrifugation at 8000 rpm for 10 min, dispersed in 50 mL methanolic solution containing 1% HCl and refluxed at 80 °C for 12 h before calcination at 500 °C for 4 h to completely remove the CTAB surfactant templates. MSNs were separated again by centrifugation, washed with distilled water and dried at 50 °C, overnight. In the final step, 20 mg MSNs and 5 mg as-prepared CDs were dispersed in 20 mL of deionized water under sonication for 10 min followed by gentle mixing at 25 °C for 24 h. The CDs incorporated MSNs (MSNs-CDs) were then separated under centrifugation and dried at 40 °C, overnight. The weight ratio of loaded CDs to the total weight of MSNs-CDs was considered as the CDs loading efficiency. MSNs-CDs were then dispersed in 1 mL of 1% (v/v) aqueous solution of acetic acid containing Ch (0.5%, w/v) under stirring at 200 rpm for 6 h. The Ch coated MSNs-CDs (MSNs-CDs-Ch) were separated under centrifugation before functionalization with anti-MUC1 aptamer, according to the previously reported procedure.[32] Briefly, 10 mg of MSNs-CDs-Ch were dispersed in 1 mL of phosphate buffer (50 mmol L^{-1}, pH 7.0) containing 2% GA and incubated under gentle stirring for 4 h. GA functionalized nanoplatforms (MSNs-CDs-Ch-GA) were then separated by centrifugation, washed with deionized water and dispersed again in 1 mL of phosphate buffer (50 mM, pH 8.5). After the addition of anti-MUC1 aptamer and 12 h incubation under gentle shaking at 25 °C, the aptamer targeted NPs (MSNs-CDs-Ch-Apt) were separated by centrifugation, washed with deionized water, and dispersed in PBS for the subsequent storage at 4 °C. The concentration of aptamer in the solution before and after the reaction was measured using an Epoch Micro-Volume Spectrophotometer (BioTek, USA) to evaluate the efficiency of aptamer binding to the NPs surface. The binding efficiency was calculated based on the ratio of the concentration of aptamers conjugated on the nanoparticles surface to the total concentration of aptamers used in the reaction.

2.3. Characterization of nanostructures

The size, shape, and elemental composition of MSNs were analyzed using a field emission scanning electron microscopy (FE-SEM, FEI ESEM Quanta 200, USA) equipped with X-ray energy dispersive spectroscopy (EDS, silicon drift detectors, Germany) at an accelerating voltage of 25 kV. Transmission electron microscopy (TEM) images were obtained by using

a JEOL 1230 transmission electron microscope. The ζ potential values and hydrodynamic sizes of CDs were measured using SZ-100 nanoparticle analyzer (Horiba, Japan). A Bruker D-8 Advance powder X-ray diffractometer (Shimadzu, Japan) with Cu Kα radiation ($\lambda = 1.5406$ Å) was used to record the X-ray diffraction (XRD) pattern of MSNs. Fourier transform infrared (FTIR) spectra were recorded using a Jasco FTIR-6300 spectrometer over the wavenumber range of 4000–400 cm^{-1}. Thermogravimetric analysis (TGA) was carried out using a Mettler TG50 (Schwerzenbach, Switzerland) from 25 °C to 700 °C at a heating rate of 10 °C min^{-1} under nitrogen atmosphere. A BELSORP-mini II instrument (Bel Japan Inc., Japan) was used to evaluate and compare the nitrogen adsorption/desorption isotherms of MSNs and MSNs-CDs. The Brunauer–Emmett–Teller (BET) method and Barrett–Joyner–Halenda (BJH) model were then used to calculate the surface area, pore size and pore volume of MSNs and MSNs-CDs from the nitrogen desorption isotherms. The release of CDs from MSNs was also studied in the simulated condition with the cancer cells. For this purpose, nanoparticles were incubated in PBS buffer (pH 5.0) and the fluorescence of supernatant was measured after 3, 6, 12, 24, 36, 48, and 72 hours.

2.4. *In vitro* studies

The biocompatibility and potential anticancer activity of nanostructures were first studied *in vitro* on the breast cancer cell lines of MCF-7 and MDA-MB-231 and the non-cancerous human umbilical vein endothelial cells (HUVEC) by MTT assay. For this purpose, 10^4 cells with 200 μL RPMI 1640 medium were added into each well of 96-well plates and incubated at 37 °C in a humidified 5% CO_2 incubator. After 24 h, the medium was discarded and different concentrations (1, 10, 50, and 100 μg mL^{-1} in media) of each NPs, including CDs, MSNs, MSNs-CDs, MSNs-CDs-CH, and MSNs-CDs-Ch-Apt, were added into the individual wells and incubated again for 48 h at the same condition. Then, the medium was completely replaced with 100 μL of MTT solution (0.5 mg mL^{-1} in media) and incubated for 4 h at the same condition. Finally, the medium was carefully discarded and the formazan crystals were dissolved in 100 μL DMSO and the absorbance was measured at 570 nm. The cell viabilities were calculated as the ratio of absorbance values from each treatment and control. The cell morphology changes were also monitored by the optical microscope. The anticancer drug of 5-FU was also used at the same condition, as the control.

The intracellular uptake efficiencies of the nanoplatforms and their potential use for fluorescence imaging were also studied, *in vitro*, using an inverted microscope system (Nikon, Eclipse Ti–U). To this aim, the cells were exposed with 10 μg mL^{-1} of MSNs-CDs-Ch-Apt for 4 h and washed with PBS buffer before fluorescence imaging.

The abundance of apoptosis and necrosis of cancer cells after exposure with the NPs were investigated by Annexin V-FITC/propidium iodide (PI) staining, according to the previous reports.[33,34] To this aim, 2×10^5 MCF-7 cells were seeded in each well of 6-well plates and incubated at 37 °C in a humidified 5% CO_2 incubator, overnight. The cells were then exposed with 50 μg mL^{-1} of MSNs-CDs-Ch-Apt for 48 h. The medium and suspended cells of each well were then completely separated and stored, individually. The remained cells were also harvested by trypsinization and added into the stored media. The cells were then precipitated completely by centrifugation at 2000 rpm for 5 min and stained according to the manufacturer's instruction (Biolegend, San Diego, CA). Briefly, the cell pellets were washed with cold staining buffer and suspended in 100 μL annexin V binding buffer containing 5 μL annexin V-FITC (100 μg mL^{-1}) and 10 μL PI solution (0.5 μg mL^{-1}). The samples were incubated for 15 min in dark condition before flow cytometric analysis using a BD FACS Calibur™ (BD Biosciences, San Jose, CA, USA) at the excitation wavelength of 488 nm. FITC was detected in FL-1 by 525/30 BP filter and PI was detected in FL-2 by 575/30 BP filter. 2×10^4 cells were used in each assay and analyzed using WinMDI 2.8 software to determine the percentages of early apoptotic (annexin V^+, PI^-), late apoptotic (annexin V^+, PI^+), necrotic (annexin V^-, PI^+) and live (annexin V^-, PI^-) cells.

2.5. Statistical analysis

All the *in vitro* experiments were carried out in triplicate and the final results were presented as the mean value ± standard deviation (SD). All statistical analyses were performed using the SPSS version 20.0 for Windows and P values of less than 0.05 were considered as the statistically significant.

3. Results and discussion

3.1. Synthesis and characterization of NPs

MSNs have been one of the most widely used drug delivery nanocarriers over the past 20 years.[35] Recently, MSNs have also attracted an increased attention for cancer therapy and imaging.[18] Development of MSNs-based theranostic nanoplatforms is another new approach of cancer research. In this context, the use of CDs as a pH-responsive gatekeeper for FRET-based monitoring of doxorubicin (DOX) release from the AS1411 aptamer-targeted magnetic MSNs have been reported by our group, recently.[32] These fluorescent CDs with high quantum yield of up to 50.4% in the wavelength range of 460–520 nm and a potent anticancer activity were also synthesized in one of our previous studies.[21] Green synthesis of CDs by using the natural compounds, such as taxanes, provides a simple and cost-effective method for the development of theranostic agents, without the use of hazardous chemicals.[21,32] Moreover, this method overcomes the problem of hydrophobicity of taxanes, which adversely affects their bioavailability in the physiological condition. The results of some characterization analyses of these CDs are presented in Fig. S1.†

The previous promising results prompted us to explore new MSNs-based nanostructures with higher CDs loading, different surface coverage, and new targeting agents in order to achieve better performances. To this aim, MSNs were synthesized using the well-known sol–gel method based on the literature,[31,36] and loaded only with CDs. The details of the reaction steps involved

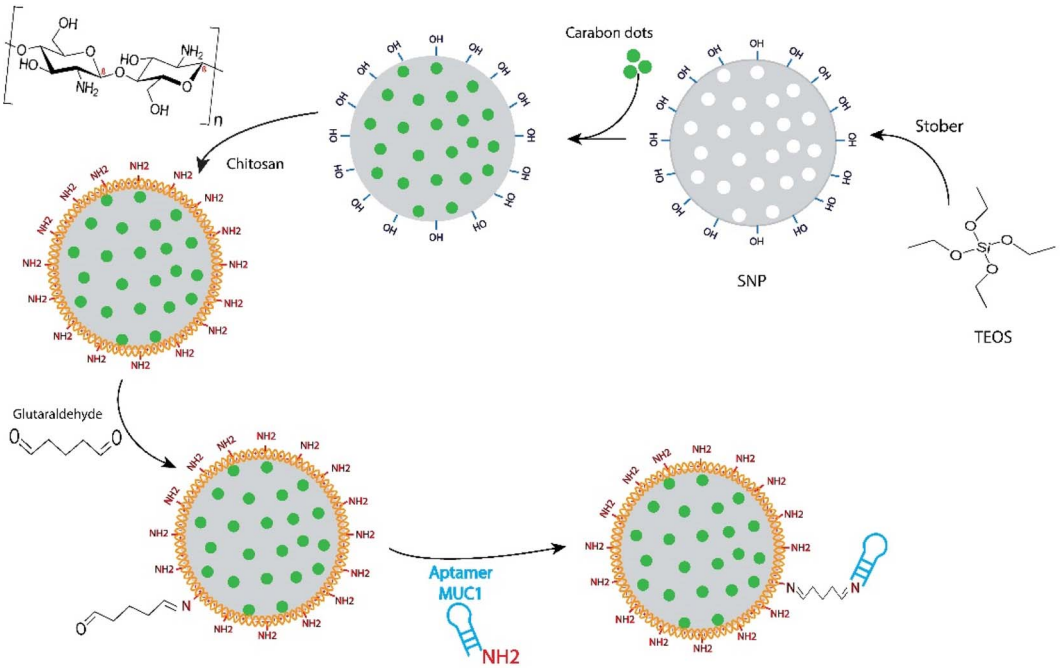

Scheme 1 Schematic representation for the synthesis procedure of CDs incorporated mesoporous silica nanoparticles targeted with anti-MUC1 aptamer.

in the development of multifunctional theranostic MSNs are shown in Scheme 1. The hydrogen bonds between hydroxyl functional groups of MSNs and CDs can be considered as the main interaction force for the CDs loading into the MSNs. A loading efficiency of 10.8% was obtained for CDs after the incubation with MSNs, under gentle mixing at 25 °C for 24 h. The surface coating of MSNs with chitosan, *via* the electrostatic interaction of positively charged amine groups of Ch with the negatively charged hydroxyl groups of MSNs, was followed to cap the mesopores as well as to provide the appropriate functional groups for the subsequent aptamer conjugation. Glutaraldehyde was used, as a crosslinker, to attach the anti-MUC1 aptamers on the surface of MSNs through the imine bonds between the aldehyde groups of the crosslinker with the primary amines of chitosan and aptamer.

The physicochemical properties of MSNs were first characterized using SEM, TEM, and XRD (Fig. 1). The results of SEM and TEM imaging indicated the synthesis of highly monodisperse MSNs with a spherical shape and approximately 50 nm size. MSNs represent the appropriate properties of the

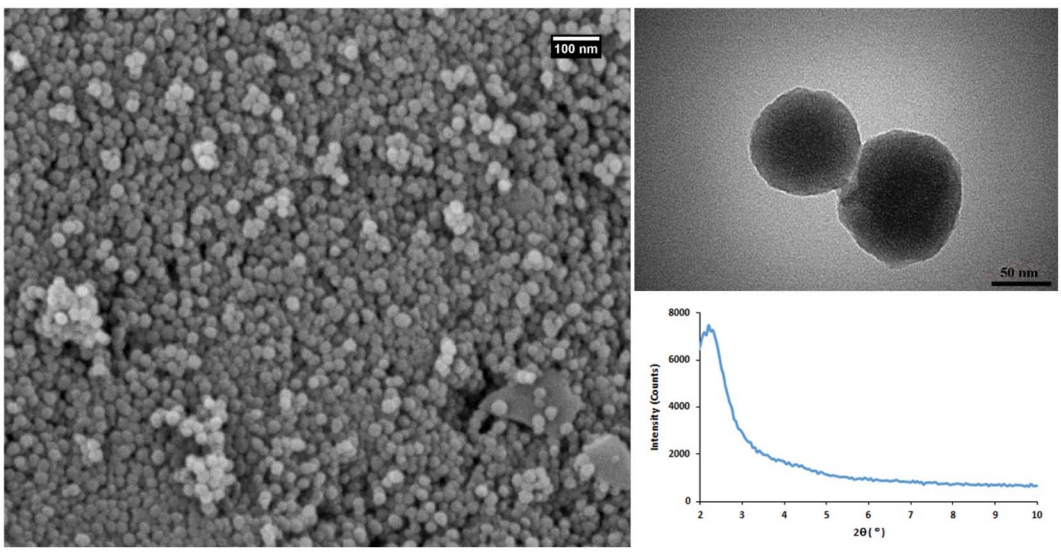

Fig. 1 The characterization results of MSNs. FE-SEM (left), TEM (right-up), and XRD (right-down), analysis.

nanocarriers for biomedical applications. The low angle XRD analysis showed a diffraction peak at 2.2° corresponding to (100) plane of MSNs.[37] EDS elemental analysis confirmed that MSNs are composed of silica and oxygen with the weight percentages of 56.13 and 43.87, respectively (Fig. S2†).

MSNs were characterized again following the CDs loading. TEM imaging clearly showed the significant incorporation of CDs and formation of a new coating layer on the MSNs surface (Fig. 2). Based on TGA analysis, up to 9.43% weight loss of MSNs-CDs obtained after air heating up to 400 °C (Fig. S3†). This observation could be attributed to the oxidative decomposition of incorporated CDs. BET analysis was used to further investigate the CDs loading of MSNs. The results of nitrogen adsorption–desorption analysis of MSNs before and after CDs loading showed the hysteresis loops (Fig. 2) corresponded to the type IV isotherm which indicates the high mesoporous nature of MSNs. The initial MSNs represent high surface area of 507.25 $m^2 g^{-1}$ while the surface area of MSNs-CDs decreased to 224.56 $m^2 g^{-1}$ indicating the significant loading of CDs. The total pore volume of MSNs after CDs loading also decreased from 1.01 $cm^3 g^{-1}$ to 0.85 $cm^3 g^{-1}$ (Fig. 2).

The resulted MSNs-CDs were then coated with Ch before targeting with the DNA aptamers. The unique characteristics of Ch biopolymer especially biodegradability, biocompatibility, and low cost, make it a preferred choice for the biomedical applications.[38] Regarding the high negative charge density of MSNs-CDs surface, due to the presence of hydroxyl, carbonyl and carboxyl groups, the surface coating could be easily obtained through the electrostatic interactions and hydrogen bonds. Based on TEM imaging, MSNs-CDs-Ch represent a semi-spherical shape with a modified surface due to the Ch coating (Fig. 2). Finally, MSNs-CDs-Ch were functionalized by GA and targeted with the anti-MUC1 aptamer, *via* the Schiff base reaction.

The functionalization of MSNs was also investigated stepwise using the FTIR spectroscopy (Fig. 3). The characteristic peaks observed at 1086, 798, and 949 cm^{-1} were assigned to the asymmetric and symmetric stretching vibrations of Si–O–Si, and stretching vibration of Si–OH, respectively, which confirm the successful synthesis of MSNs.[14,39] The broad band located around 3423 cm^{-1} is attributed to the typical stretching vibrations of O–H and N–H bonds.[40] The peak observed at 1625 cm^{-1} was also assigned to the OH stretching vibrations.[41] The absorption band at 1454 cm^{-1} was ascribed to the C–H bending vibration.[39] The appearance of the C–H stretching bands at 2863 and 2935 cm^{-1} in MSNs-CDs indicated the successful incorporation of CDs.[42] The newly appeared stretching vibration bands at 1362 cm^{-1} was also attributed to the amine groups of Ch.[14] The absorption band at 1525 cm^{-1} was assigned to the vibrations of N–H bond of amino groups.[43] These data indicate the successful coating of MSNs-CDs with Ch. The appeared peak at 1713 cm^{-1} after surface functionalization with GA is attributed to the stretching vibration of carbonyl groups.[41] The appearance of new peak at 1671 cm^{-1} corresponds to the imine (C=N) bonds, resulted by Schiff base reaction between the primary amine group of Ch and carbonyl groups of GA.[40]

To improve the specificity of NPs toward the cancer cells and also to improve their cell internalization efficiency, in the last step, NPs were functionalized by anti-MUC1 aptamer. The active targeting of NPs toward the cells *via* the specific ligands, such as antibodies and DNA aptamers, has greatly considered, recently.[44] The significant advantages of DNA aptamers over the

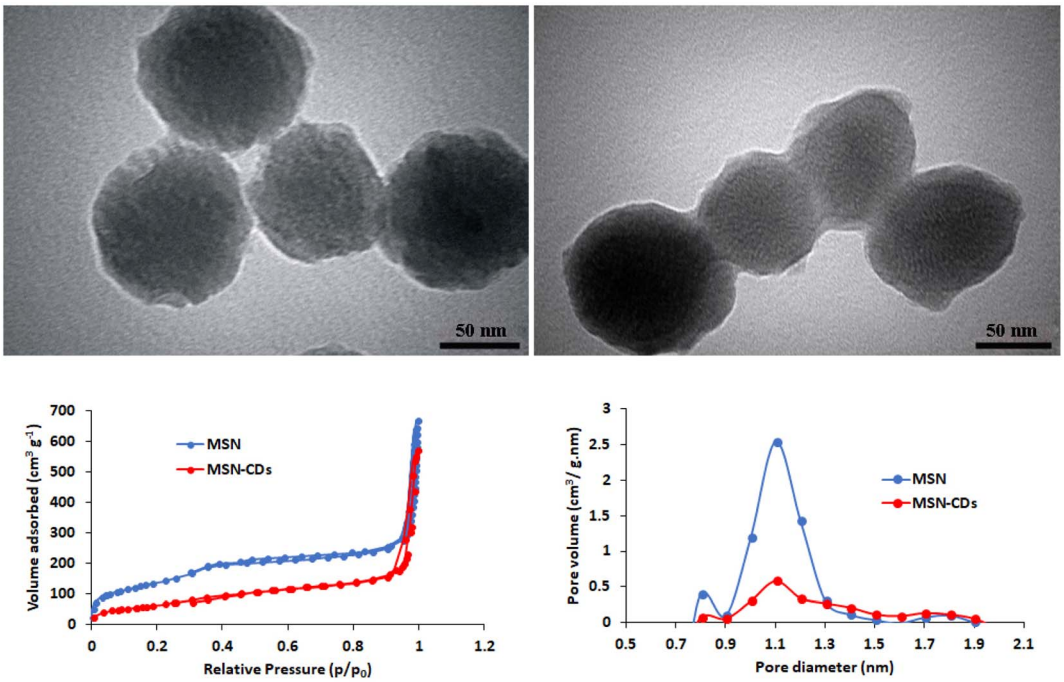

Fig. 2 TEM images of MSNs-CDs (left up) and MSNs-CDs-Ch (right up). The nitrogen adsorption–desorption isotherms (left bottom) and pore diameter/pore volume (right bottom) of MSNs and MSNs-CDs.

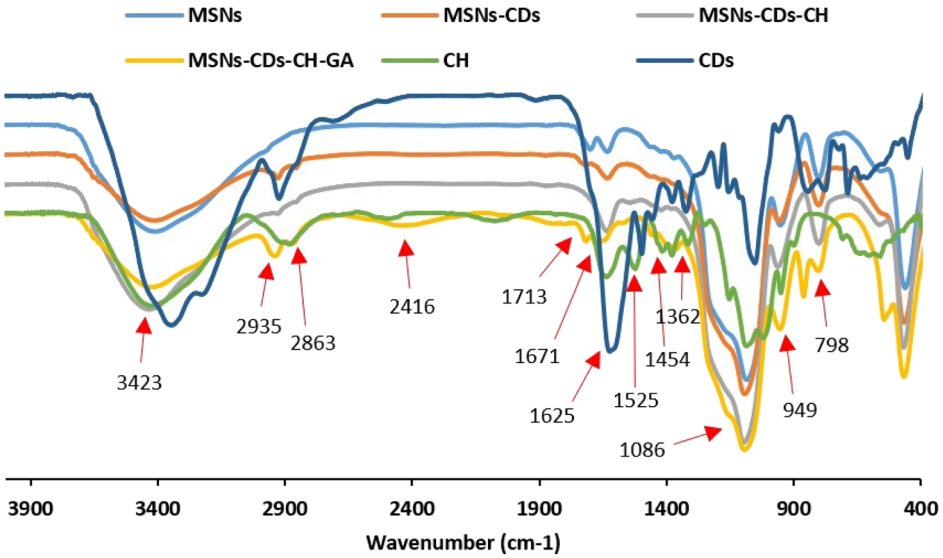

Fig. 3 FTIR analysis of MSNs functionalization, including CDs, CH, MSNs, MSNs-CDs, MSNs-CDs-Ch and MSNs-CDs-Ch-GA.

antibodies, especially low cost, easy synthesis and modification, high stability and comparable affinity, led to their increased application.[45] In the present study, anti-MUC1 aptamer was used to target the CDs incorporated MSNs toward the breast cancer cells. MUC1 receptor is mainly overexpressed on the surface of human epithelial cancer cells.[46,47] A previously reported specific and short (25-bp) DNA aptamer with high affinity (K_d value of 0.135 nM) for MUC1 receptor was used for this purpose.[30] The amine-terminated aptamers were easily conjugated to the amine groups of Ch on the MSNs surface *via* the GA linkers. This simple, fast and mild reaction also prevents the potential damage or deformation of DNA aptamers during the conjugation. The concentration of DNA aptamer in the supernatant, after the reaction, was 14.6 μg mL^{-1} while the total amount of aptamers used in the reaction was 98.7 μg mL^{-1}. Therefore, the binding efficiency of aptamer to the NPs surface was 85.21%. Considering the total amount of the conjugated aptamers (84.1 μg) on the functionalized MSNs (10 mg), the concentration of aptamer on the surface of final nanostructure (MSNs-CDs-Ch-Apt) was calculated to be about 8.41 μg mg^{-1}.

3.2. *In vitro* studies

To investigate the potential anticancer activity of nanostructures, a comprehensive MTT assay was first conducted *in vitro*. The toxicity of nanoplatforms, including CDs, MSNs, MSNs-CDs, MSNs-CDs-Ch, and MSNs-CDs-Ch-Apt, as well as the anticancer drug of 5-FU, was studied on MCF-7 and MDA-MB-231 breast cancer cells and the normal HUVEC cells. MSNs represented the negligible cytotoxicity on all three cell lines, indicating their high biocompatibility and therefore, their high potential as the nanocarrier (Fig. 4). The biocompatibility of MSNs, as an ideal drug delivery nanocarrier, has been extensively studied and reported, recently.[48–50] MSNs-CDs, in contrast to MSNs, represent the highest cytotoxicity on all the studied cell lines. The results of statistical analysis showed that the anticancer effect of MSNs-CDs, on both cancer cell lines, is significantly higher than the free CDs. The exposure of MCF-7, MDA-MB-231, and HUVEC cells with 100 μg mL^{-1} MSNs-CDs for 48 h exposure led to 87.93 ± 2.55, 85.82 ± 2.68, and 88.35 ± 1.77% mortality, respectively (Fig. 4A).

The optical microscopy imaging of MCF-7 cancer cells after exposure with MSNs-CDs also confirmed the considerable change in the morphology and inhibition of growth, which indicates the high cellular toxicity of MSNs-CDs (Fig. S4†). With regards to the biocompatible nature of MSNs, this observation could be attributed to the cytotoxicity of CDs. In the previous study, IC_{50} value of 82.1 ± 4 μg mL^{-1} was obtained after 48 h exposure of MCF-7 cells to CDs. Since CDs constitute only about 10% of the total weight of MSN-CDs, the present results show that the use of MSNs for delivery of CDs has multiplied their anticancer activity. The loading of CDs into MSNs can also keep them away from the additional reactions with the medium components. The observed cytotoxicity of MSNs-CDs was even higher than our previously reported magnetic MSNs incorporated with DOX and CDs.[32] The high cytotoxicity of MSNs-CDs, developed in the present study, could be attributed to the higher loading of CDs into MSNs. Since no magnetic NPs was incorporated in the present MSNs, they have more loading capacity for anticancer CDs, which can lead to the higher anticancer activity of resulted MSNs-CDs. Moreover, the lack of appropriate surface coating can also lead to the faster release of CDs from MSNs and thus, the greater cytotoxicity of MSNs-CDs. Owing to the non-specific cytotoxicity of MSNs-CDs, their surface modification and targeting against cancer cells is essential.

For this purpose, MSNs-CDs surface was first coated with the biocompatible and biodegradable Ch polymer. Based on the results (Fig. 4A), the Ch coating of MSNs-CDs significantly decreased the cytotoxicity of MSNs-CDs, possibly due to the controlled release of CDs. The subsequent functionalization of MSNs-CDs-Ch with the anti-MUC1 aptamer, led to the further

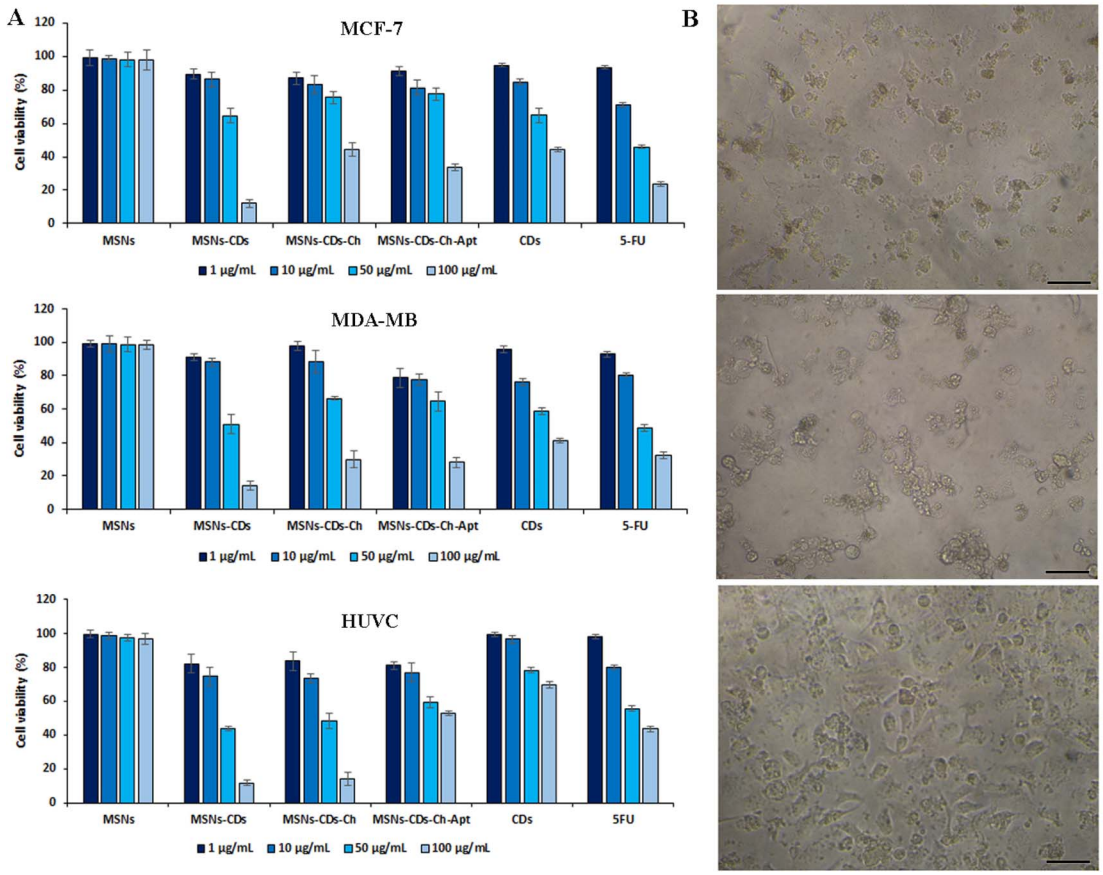

Fig. 4 *In vitro* cell studies. (A) The viability percentage of MCF-7, MDA-MB-231 and HUVEC cells after 48 h exposure with different concentrations of MSNs, MSNs-CDs, MSNs-CDs-Ch and MSNs-CDs-Ch-Apt, CSs, 5-FU, and (B), optical microscopy images of the cells after 48 h exposure with 100 μg mL^{-1} MSNs-CDs-Ch-Apt (scale bars = 50 μm).

increase of the anticancer activity without the significant effect on the non-specific toxicity of nanoplatforms on the normal HUVEC cells. Therefore, the Ch coating and aptamer targeting of MSNs-CDs led to the potent and specific anticancer activity. In this condition, the maximum cell mortalities of 66.2 ± 1.97 and 71.8 ± 3% obtained for MCF-7 and MDA-MB-231 cells, respectively, after 48 h exposure with 100 μg mL^{-1} MSNs-CDs-Ch-Apt (Fig. 4A). The exposure with 100 μg mL^{-1} CDs for 48 h, at the same condition, led to the cell mortalities of 55.69 ± 1.58 and 58.63 ± 1.38% in MCF-7 and MDA-MB-231 cells, respectively. Considering the loading efficiency of CDs in the MSNs (10.8%), these results indicate a considerably higher anticancer activity of MSNs-CDs-Ch-Apt. The results were comparable with the obtained cell mortalities of 76.31 ± 1.46 and 67.61 ± 1.92% for MCF-7 and MDA-MB-231 cells, respectively, after 48 h exposure with 100 μg mL^{-1} of anticancer drug, 5-FU. At the same condition, 40.66 ± 1.3% mortality of HUVEC cells was observed, after 48 h exposure with 100 μg mL^{-1} MSNs-CDs-Ch-Apt. The results were comparable with the previously reported mortality of 65.71% after 48 h exposure of MCF-7 cells with 100 μg mL^{-1} magnetic MSNs incorporated with CDs and DOX.[32]

Regarding the potential adverse effects of GA on the cells and human health, such as the induction of respiratory irritation, neurotoxicity, oxidative stress, and inflammation,[51,52] the *in vitro* cell studies of GA functionalized MSNs are also important for the biomedical applications. Based on the results of MTT assay, no increased mortality of HUVEC cells was observed after the exposure with MSNs-CDs-Ch-Apt that indicates the absence of adverse effects of GA on the final nanoplatform. Since the adverse effects of GA have been reported to be dose-dependent,[52] this result could be due to the use of low concentrations of GA. Moreover, as the behavior of GA in the solution is affected by its structure,[53] the crosslinked GA is expected to represents different biological effects than the free GA. The overall results indicate more selective anticancer activity of aptamer-functionalized MSNs than the initial NPs. The results of MTT assay were also confirmed by the microscopic imaging of cell morphology changes after exposure with MSNs-CDs-Ch-Apt (Fig. 4B).

The time-dependent release of CDs from MSNs was studied by using the fluorescence spectroscopy. As illustrated in Fig. S5,† a significant release of CDs occurred during the first 24 hours of incubation, after which the fluorescence changes decreased significantly.

The potential use of MSNs-CDs-Ch-Apt for the fluorescence imaging of cancer cells was also studied *in vitro*. Based on the results (Fig. 5A), the appropriate fluorescence imaging of MCF-7

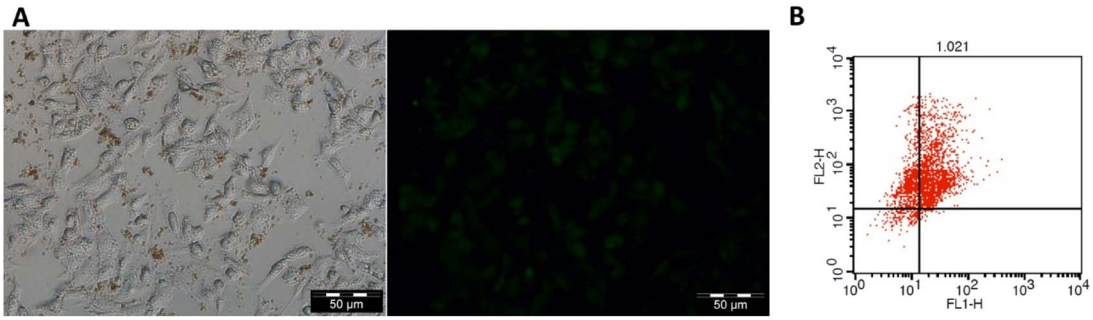

Fig. 5 *In vitro* optical (A) and fluorescence (B) imaging of MCF-7 cells exposed with MSNs-CDs-Ch-Apt for 24 h (A). Flow cytometry analysis of apoptosis and necrosis in MCF-7 cells after 48 h exposure with 50 μg mL^{-1} of MSNs-CDs-Ch-Apt (B).

cells obtained after 24 h exposure with MSNs-CDs-Ch-Apt. The overall results indicate high potential of developed nanoplatform, as a cancer theranostic agent, for the simultaneous imaging and targeted cancer therapy.

The anticancer activity of CDs and MSNs-CDs-Ch-Apt was further studied by using flow cytometry analysis. For this purpose, MCF-7 cells were stained with annexin V-FITC and PI after 48 h exposure to 50 μg mL^{-1} concentration of CDs and MSNs-CDs-Ch-Apt. In this condition, the over-expressed phosphatidylserine molecules on the surface of apoptotic cells are expected to be recognized by annexin V proteins while PI selectively inters the late apoptotic and necrotic cells and intercalates with the nuclear DNA.[54] Flow cytometry analysis of stained cells showed that 64.7 and 26.54% of MCF-7 cells are in the late apoptotic and necrotic stages, respectively. Only 6.65% of cells were still alive while the remaining 2.11% were in the early apoptotic stage. Therefore, the results of MTT assay were further confirmed and late apoptosis was identified as the main cause of cell death (Fig. 5B). Similarly, the exposure of MCF-7 cells with CDs at the same condition for 48 h led to the late apoptosis of 81.85% of cells while 13.07% of cells were in the early apoptosis stage. These results are also consistent with our previous data about the anticancer mechanism of CDs, *via* the induction of apoptosis.

4. Conclusion

The growing number of cancer patients in the world and the lack of a definitive treatment strategy for this disease have raised many concerns. One of the main limitations is the side effects of most common chemotherapeutic agents. The use of biogenic approach for development of novel cancer therapeutics with the superior activities and less side effects has been greatly considered to address this limitation. The use of non-toxic materials and solvents for synthesis of chemotherapeutics could also significantly reduce their potential toxicity and side effects. The targeted delivery by using biocompatible and biodegradable NPs, such as MSNs, is another strategy to overcome the obstacles of cancer therapy. Both approaches of biogenic synthesis and targeted delivery were considered in the present study. Accordingly, the targeted and controlled delivery of green synthesized CDs, with the potent anticancer and fluorescence activities, obtained by the aptamer-functionalized MSNs. The resulted theranostic nanoplatforms showed a high anticancer activity, comparable to the anticancer activities obtained previously by the combined use of CDs and anticancer drugs. The targeted delivery of CDs was also used for the fluorescence imaging of cancer cells. The theranostic nanoplatforms were developed merely by using the biogenic precursors and green methods. The use of biocompatible MSNs, as a drug delivery carrier, and their appropriate functionalization and the aptamer targeting, led to the improved anticancer effects on the cancer cells while significantly inhibited the non-specific effects of nano-therapeutic agents on the normal cells. The surface coating of NPs with the biocompatible and biodegradable Ch was used as a simple and efficient approach for the controlled release of cargos and also their subsequent functionalization. The aptamer targeting against cancer cells was a simple and cost-effective method to inhibit nonselective cytotoxicity of nanostructures. Therefore, this rationally designed multifunctional nanoplatform represents high potential for the simultaneous cancer therapy and fluorescence imaging.

Abbreviations

BET	Brunauer–Emmett–Teller
BJH	Barrett–Joyner–Halenda
CDs	Carbon dots
Ch	Chitosan
CTAB	Cetyltrimethylammonium bromide
CTCs	Circulating tumor cells
DLS	Dynamic light scattering
DMSO	Dimethyl sulfoxide
DOX	Doxorubicin
EDS	Energy dispersive X-ray spectroscopy
FBS	Fetal bovine serum
FE-SEM	Field emission scanning electron microscopy
FTIR	Fourier transform infrared spectroscopy
GA	Glutaraldehyde
HUVEC	Human umbilical vein endothelial cells
LMW	Low molecular weight
MCF-7	Michigan cancer foundation-7
MDA-MB	M. D. Anderson metastasis breast
*m*PDA	*m*-Phenylenediamine

MSNs	Mesoporous silica nanoparticles
MSNs-CDs	CDs loaded MSNs
MSNs-CDs-Ch	Chitosan coated MSNs-CDs
MSNs-CDs-Ch-Apt	Aptamer targeted MSNs-CDs-Ch
MSNs-CDs-Ch-GA	Glutaraldehyde functionalized MSNs-CDs-Ch
MTT	3-(4,5-Dimethylthiazol-2-yl)-2,5-diphenyltetrazolium bromide
MUC1	Mucin 1
NPs	Nanoparticles
PBS	Phosphate buffered saline
PI	Propidium iodide
RPMI	Roswell park memorial institute
SD	Standard deviation
TEM	Transmission electron microscopy
TEOS	Tetraethyl orthosilicate
TGA	Thermogravimetric analysis
UV-vis	Ultraviolet-visible
XRD	X-Ray diffraction

Author contributions

Abolghasem Abbasi Kajani: conception, design, analysis and writing of the study. Laleh Rafiee: analysis and writing of the study. Shaghayegh Haghjooy Javanmard: conception and design of the study. Nasim Dana: analysis and writing of the study. Setareh Jandaghian: analysis of the study.

Conflicts of interest

The authors declare no conflict of interest.

Acknowledgements

The financial supports of Isfahan University of Medical Sciences are gratefully acknowledged.

References

1 H. Sung, J. Ferlay, R. L. Siegel, M. Laversanne, I. Soerjomataram, A. Jemal, F. Bray and C. A. Cancer, *Ca-Cancer J. Clin.*, 2021, **71**, 209–249.
2 L. Wu, Y. Wang, L. Zhu, Y. Liu, T. Wang, D. Liu, Y. Song and C. Yang, *ACS Appl. Bio Mater.*, 2020, **3**, 2743–2764.
3 H. Li, Q. Yao, W. Sun, K. Shao, Y. Lu, J. Chung, D. Kim, J. Fan, S. Long, J. Du, Y. Li, J. Wang, J. Yoon and X. Peng, *J. Am. Chem. Soc.*, 2020, **142**, 6381–6389.
4 P. Bhattarai, S. Hameed and Z. Dai, *Nanoscale*, 2018, **10**, 5393–5423.
5 A. Abbasi Kajani, A. K. Bordbar, S. H. Zarkesh-Esfahani, A. Razmjou and J. Hou, *J. Mol. Liq.*, 2017, **247**, 238–245.
6 V. S. Madamsetty, A. Mukherjee and S. Mukherjee, *Front. Pharmacol.*, 2019, **10**, 1–12.
7 P. N. Navya, A. Kaphle, S. P. Srinivas, S. K. Bhargava, V. M. Rotello and H. K. Daima, *Nano Converg.*, 2019, **6**, 23.
8 Y. Zhou, G. Quan, Q. Wu, X. Zhang, B. Niu, B. Wu, Y. Huang, X. Pan and C. Wu, *Acta Pharm. Sin. B*, 2018, **8**, 165–177.
9 D. Wang, H. Wu, S. Z. F. Phua, G. Yang, W. Qi Lim, L. Gu, C. Qian, H. Wang, Z. Guo, H. Chen and Y. Zhao, *Nat. Commun.*, 2020, **11**, 1–13.
10 M. Xuan, J. Shao, J. Zhao, Q. Li, L. Dai and J. Li, *Angew. Chem. Int. Ed.*, 2018, **57**, 6049–6053.
11 Z. Yang, W. Fan, J. Zou, W. Tang, L. Li, L. He, Z. Shen, Z. Wang, O. Jacobson, M. A. Aronova, P. Rong, J. Song, W. Wang and X. Chen, *J. Am. Chem. Soc.*, 2019, **141**, 14687–14698.
12 A. Aghebati-Maleki, S. Dolati, M. Ahmadi, A. Baghbanzhadeh, M. Asadi, A. Fotouhi, M. Yousefi and L. Aghebati-Maleki, *J. Cell. Physiol.*, 2020, **235**, 1962–1972.
13 H. D. M. Follmann, O. N. Oliveira, D. Lazarin-Bidóia, C. V. Nakamura, X. Huang, T. Asefa and R. Silva, *Nanoscale*, 2018, **10**, 1704–1715.
14 M. S. Moorthy, G. Hoang, P. Manivasagan, S. Mondal, T. T. Vy Phan, H. Kim and J. Oh, *J. Porous Mater.*, 2019, **26**, 217–226.
15 Y. Gao, S. Zhong, L. Xu, S. He, Y. Dou and S. Zhao, *Microporous Mesoporous Mater.*, 2019, **278**, 130–137.
16 M. Aquib, M. A. Farooq, P. Banerjee, F. Akhtar, M. S. Filli, K. O. Boakye-Yiadom, S. Kesse, F. Raza, M. B. J. Maviah, R. Mavlyanova and B. Wang, *J. Biomed. Mater. Res., Part A*, 2019, **107**, 2643–2666.
17 N. Shadjou and M. Hasanzadeh, *J. Biomed. Mater. Res., Part A*, 2015, **103**, 3703–3716.
18 P. Kumar, P. Tambe, K. M. Paknikar and V. Gajbhiye, *J. Control. Release*, 2018, **287**, 35–57.
19 H. Ding, X. Zhou, B. Qin, Z. Zhou and Y. Zhao, *J. Lumin.*, 2019, **211**, 298–304.
20 B. Yang, H. Chen, Z. Zheng and G. Li, *J. Lumin.*, 2020, **223**, 117226.
21 A. Abbasi Kajani, A. K. Bordbar, M. A. Mehrgardi, S. H. Zarkesh-Esfahani, H. Motaghi, M. Kardi, A. R. Khosropour, J. Ozdemir, M. Benamara and M. H. Beyzavi, *ACS Appl. Bio Mater.*, 2018, **1**, 1458–1467.
22 Y. Li, G. Bai, S. Zeng and J. Hao, *ACS Appl. Mater. Interfaces*, 2019, **11**, 4737–4744.
23 L. F. Ornelas-Hernández, A. Garduno-Robles and A. Zepeda-Moreno, *Nanoscale Res. Lett.*, 2022, **17**, 56.
24 K. Wang, H. Yao, Y. Meng, Y. Wang, X. Yan and R. Huang, *Acta Biomater.*, 2015, **16**, 196–205.
25 M. S. Kang, R. K. Singh, T. H. Kim, J. H. Kim, K. D. Patel and H. W. Kim, *Acta Biomater.*, 2017, **55**, 466–480.
26 S. Zhao, S. Sun, K. Jiang, Y. Wang, Y. Liu, S. Wu, Z. Li, Q. Shu and H. Lin, *Nano-Micro Lett.*, 2019, **11**, 1–13.
27 Y. Wang, W. Shi, S. Wang, C. Li, M. Qian and J. Chen, *Carbon*, 2016, **108**, 146–153.
28 Y. Y. Liu, N. Y. Yu, W. Di Fang, Q. G. Tan, R. Ji, L. Y. Yang, S. Wei, X. W. Zhang and A. J. Miao, *Nat. Commun.*, 2021, **12**, 1–12.
29 N. Esfandiari, Z. Bagheri, H. Ehtesabi, Z. Fatahi, H. Tavana and H. Latifi, *Heliyon*, 2019, **5**, e02940.
30 C. S. M. Ferreira, C. S. Matthews and S. Missailidis, *Tumor Biol.*, 2006, **27**, 289–301.

31 Y. J. Cheng, A. Q. Zhang, J. J. Hu, F. He, X. Zeng and X. Z. Zhang, *ACS Appl. Mater. Interfaces*, 2017, **9**, 2093–2103.
32 A. Abbasi Kajani and M. Ayatollahi Mehrgardi, *Nanomedicine*, 2021, **16**, 627–639.
33 A. Abbasi Kajani, A. K. Bordbar, S. H. Zarkesh-Esfahani and A. Razmjou, *RSC Adv.*, 2016, **6**, 63973–63983.
34 A. Abbasi Kajani, S. H. Zarkesh-Esfahani, A. K. Bordbar, A. R. Khosropour, A. Razmjou and M. Kardi, *J. Mol. Liq.*, 2016, **223**, 549–556.
35 X. Yang, D. He, X. He, K. Wang, J. Tang, Z. Zou, X. He, J. Xiong, L. Li and J. Shangguan, *ACS Appl. Mater. Interfaces*, 2016, **8**, 20558–20569.
36 M. D. Yilmaz, *Carbohydr. Polym.*, 2016, **146**, 174–180.
37 S. Kanugala, S. Jinka, N. Puvvada, R. Banerjee and C. G. Kumar, *Sci. Rep.*, 2019, **9**, 1–16.
38 D. H. Kim, K. N. Kim, K. M. Kim and Y. K. Lee, *J. Biomed. Mater. Res., Part A*, 2009, **88**, 1–11.
39 K. Panwar, M. Jassal and A. K. Agrawal, *Particuology*, 2015, **19**, 107–112.
40 Z. A. Sutirman, M. M. Sanagi, K. J. Abd Karim and W. A. Wan Ibrahim, *Carbohydr. Polym.*, 2016, **151**, 1091–1099.
41 F. Chen and Y. Zhu, *Microporous Mesoporous Mater.*, 2012, **150**, 83–89.
42 X. Zhu and C. Q. Wang, *J. Colloid Interface Sci.*, 2016, **480**, 39–48.
43 Y. Antsiferova, N. Sotnikova and E. Parfenyuk, *Biomed Res. Int.*, 2013, **2013**, 924362.
44 F. Maghsoudinia, M. Bagher, R. Kamran, S. Hossein, T. Sobhani, F. Mehradnia and M. A. Mehrgardi, *Talanta*, 2021, **228**, 122245.
45 H. Safarpour, S. Dehghani, R. Nosrati, N. Zebardast, M. Alibolandi, A. Mokhtarzadeh and M. Ramezani, *Biosens. Bioelectron.*, 2020, **148**, 111833.
46 B. L. Santini, M. Zúñiga-Bustos, A. Vidal-Limon, J. B. Alderete, S. A. Águila and V. A. Jiménez, *J. Chem. Inf. Model.*, 2019, **60**, 786–7933.
47 M. S. Nabavinia, A. Gholoobi, F. Charbgoo, M. Nabavinia, M. Ramezani and K. Abnous, *Med. Res. Rev.*, 2017, **37**, 1518–1539.
48 F. Mohamed, M. K. Oo, B. Chatterjee and B. Alallam, *Front. Pharmacol.*, 2022, **13**, 1–7.
49 A. Barkat, S. Beg, S. K. Panda, K. S Alharbi, M. Rahman and F. J. Ahmed, *Semin. Cancer Biol.*, 2021, **69**, 365–375.
50 R. M. Sábio, A. B. Meneguin, A. Martins dos Santos, A. S. Monteiro and M. Chorilli, *Microporous Mesoporous Mater.*, 2021, **312**, 110774.
51 Y. Wang, Q. Wu, B. Ren, L. Muskhelishvili, K. Davis, R. Wynne, D. Rua and X. Cao, *Int. J. Mol. Sci.*, 2022, **23**, 12118.
52 H. N. Oh, D. Yoo, S. Park, S. Lee and W. K. Kim, *Ecotoxicol. Environ. Saf.*, 2022, **242**, 113891.
53 W. Wan, Y. Lin, A. Prakash and Y. Zhou, *J. Mater. Chem. A*, 2016, **4**, 18687–18705.
54 S. L. Fink and B. T. Cookson, *Infect. Immun.*, 2005, **73**, 1907–1916.